1-28-2023

Harmonic Distortion Reduction of Transformer-Less Grid-Connected Converters by Ellipsoidal-Based Robust Control

Hisham M. Soliman
Faculty of Engineering

Ashraf Saleem
Michigan Technological University, ashraf@mtu.edu

Ehab H.E. Bayoumi
Faculty of Engineering

Michele De Santis
Niccolò Cusano University

Recommended Citation

Soliman, H., Saleem, A., Bayoumi, E., & De Santis, M. (2023). Harmonic Distortion Reduction of Transformer-Less Grid-Connected Converters by Ellipsoidal-Based Robust Control. *Energies, 16*(3).
http://doi.org/10.3390/en16031362
Retrieved from: https://digitalcommons.mtu.edu/michigantech-p/16890

Follow this and additional works at: https://digitalcommons.mtu.edu/michigantech-p

 Part of the Computer Sciences Commons

energies

MDPI

Article

Harmonic Distortion Reduction of Transformer-Less Grid-Connected Converters by Ellipsoidal-Based Robust Control

Hisham M. Soliman [1], Ashraf Saleem [2], Ehab H. E. Bayoumi [3] and Michele De Santis [4,*]

[1] Department of Electrical Power Engineering, Faculty of Engineering, Cairo University, Cairo 12613, Egypt
[2] Department of Applied Computing, College of Computing, Michigan Technological University, Houghton, MI 12613, USA
[3] Department of Mechanical Engineering, Faculty of Engineering, The British University in Egypt, Cairo 11837, Egypt
[4] Department of Engineering, Niccolò Cusano University, 00166 Roma, Italy
* Correspondence: michele.desantis@unicusano.it

Abstract: A photovoltaic generator connected to a large network and supplying a nonlinear load (source of harmonics) injects distorted current into the grid. This manuscript presents an invariant-ellipsoid set design of a robust controlled active power filter to inject current into the large grid with minimum total harmonic distortion (THD). The nonlinear load current is considered an external disturbance to minimize its effect on the injected grid current. Moreover, the large grid is modeled as a fixed voltage source in a series with a Thevenin impedance whose value changes within an interval. Using the invariant-ellipsoid technique, the problem is cast as a robust disturbance-rejection tracking control. The volume of the ellipsoid is minimized, which results in minimizing the effect of disturbance on system performance and keeping the trajectories as close as possible to the origin. The design is cast into a set of nonlinear matrix inequalities that are linearized by fixing a scalar. The resulting convex optimization is solved iteratively by linear matrix inequalities (LMIs). The simulation and experimental findings show that the proposed design is successful in reducing THD injected into the grid when grid impedance is uncertain and variable loads are applied (balanced and unbalanced cases).

Keywords: active power filter; invariant ellipsoid; linear matrix inequalities; robust control

Citation: Soliman, H.M.; Saleem, A.; Bayoumi, E.H.E.; De Santis, M. Harmonic Distortion Reduction of Transformer-Less Grid-Connected Converters by Ellipsoidal-Based Robust Control. *Energies* **2023**, *16*, 1362. https://doi.org/10.3390/en16031362

Academic Editor: Abu-Siada Ahmed

Received: 10 January 2023
Revised: 24 January 2023
Accepted: 26 January 2023
Published: 28 January 2023

1. Introduction

1.1. Motivation

The continuous growth of renewable energy sources, such as wind and photovoltaic power generation, has become mandatory. This is due to the increasing loads of traditional power systems as well as emerging environmental issues. Power electronics provide an interface between renewable energy sources and the grid. It enables the control of the power flow, currents, voltages, and frequencies. Such interface and nonlinear loads are the main sources of harmonics in current and voltage [1]. Therefore, grid-connected converters such as inverters and filters (for the reduction of harmonics injected into the grid) have great importance in connecting grids. For grid-connected operation, these converters have to ensure that the current injected into the grid does not violate the standards given in [2]. These standards define the permissible limits in terms of total harmonic distortion despite heavy or light-loaded grid conditions (resulting in uncertain grid impedance). The inverters are classified as either current source or voltage source inverters depending on whether the inverter is fed by a constant current or constant voltage. While only the output current magnitude of a current source inverter (CSI) drive can be adjusted, both the magnitude and frequency can be adjusted in a voltage source inverter (VSI). Therefore, VSI is commonly used in industry and is implemented in this study.

1.2. Related Research

Passive or active power filters are used for harmonic distortion reduction. Active power filters (APFs) are power electronic-based devices that provide improved filtering performance, faster response, greater flexibility, and a smaller size than passive filters. Improving power factors and voltage waveforms for single- and three-phase AC systems with nonlinear loads can be achieved by APFs [3]. Due to their cost-effectiveness and advancements in digital control techniques, APFs are widely employed in the industry for harmonic and reactive power compensation [2]. In the literature, different single-phase APF setups are presented, such as the active series filter (series with the source of harmonics) [4], active shunt filter (parallel with the source of harmonics), universal APF, and hybrid filter.

The voltage produced by VSI that is operated by a pulse width modulated (PWM) needs to be filtered to prevent grid currents that have prohibitive harmonic content. Using low-pass LCL passive filters with a rectifier input stage should reduce the harmonics of the current absorbed by power converters. However, these filters might offer poor performance and instability because of the resonance peak. These resonance peaks can be significantly reduced by inserting resistive elements into the LCL filter while considering the optimization constraints [5,6]. This method should provide a stable response but can deteriorate the system's efficiency. One possible solution is using the active damping approach [7–11]. However, a common drawback in using active damping is that the robustness to grid parameter uncertainty variations in the grid impedance is ensured posteriorly. Linear matrix inequalities (LMIs) are a useful design tool that is widely utilized to construct robust controllers that can handle parametric uncertainties and variations, especially the ones that are based on Lyapunov functions [12,13]. In grid-connected converters, LMI-based conditions allow controller synthesis while dealing with pole location and optimization constraints [14,15].

Another method that is widely used for optimal rejection of disturbances is H_1 state feedback [16]. The main drawback of this technique is the impracticality when using PWM inverters due to its high control gains, which require high-frequency components and lead to amplitude saturation. To overcome this problem, suboptimal H_1 controllers were developed where the problem of actuator saturation was mitigated by adding constraints on the size of the control gains.

Nevertheless, H_1 state feedback controllers are still not applied widely to grid-connected converters that are subject to parameter uncertainty. In [17], H_1 state feedback controllers are successfully applied on uninterruptible power supplies, with total harmonic distortion (THD) matched by a pertinent standard. In grid-connected converters, H_2 control is applied, and experimental verification is given in [18] to achieve robust control, despite the fact that grid variations and rejecting broad-band frequency disturbance exist. H∞ control is also presented in [19] to obtain optimal disturbance rejection control, robust against grid uncertainty. [20] proposes a predictive current control method based on the composite sliding mode to enhance system disturbance attenuation; however, the controller is nonlinear and time-variant.

1.3. Contributions

In this paper, the control region is modeled as an ellipsoid and the target is to attract the state trajectory of the system $x(t)$ to a small region around the origin. This method is a time-invariant method where the volume of the attracting ellipsoid is minimized while keeping the trajectory inside it for a future time.

In the proposed robust controller, the system performance (in terms of asymptotic stability, $x(t) \rightarrow 0$ as $t \rightarrow \infty$) is optimized despite any external disturbances. The research methodology and contributions of this paper can be summarized as follows:

- A linearized mathematical model is developed for a study system. The study system is a PV source and inverter + filter supplying a large grid and a nonlinear load.
- The harmonics injected into the grid current by the nonlinear load are modeled as an external disturbance to be rejected by the proposed control.

- The designed control is based on the attracting ellipsoid method (AEM), extended to the tracking problem, and LMI optimization. The controller is also robust against changes in the grid topology.
- The proposed ellipsoidal design is recently developed in robust control theory. It is utilized here for the first time to reduce the harmonics produced by the converters.
- The proposed controller in this study is proved, through simulation and experimental tests, to lower the total harmonic distortion (THD). The comparison to existing control methods shows superior performance.
- Many simulations and experimental tests are conducted to test the proposed controller: before/after adding APF, load changes, with unbalanced linear load, uncertainty grid parameters, and the distorted grid voltage.
- Unlike the other approaches, the proposed design is state feedback (proportional) control time-invariant, easy to implement, and robust against parameter uncertainties.

1.4. Paper Organization

The rest of the paper is organized as follows. Section 2 presents the problem statement and the system model. The proposed controller design is discussed in Section 3. Simulation and experimental validation are given in Section 4. Finally, Section 5 concludes the paper.

Notations

The notations are standard. R^m is the set of vectors of $m \times 1$ dimension, R^{rxq} is the set of real matrices of dimension $r \times q$, and $(.)'$ denotes the transposition of a vector or a matrix. For a matrix P, $P > 0$ (<0) means that P is a symmetric positive (negative) definite matrix. Similarly, $(M + N + *)$ means $(M + N + M' + N')$.

$$\text{A matrix } \begin{bmatrix} M & N \\ * & Z \end{bmatrix} \text{ means } \begin{bmatrix} M & N \\ N\prime & Z \end{bmatrix}.$$

Finally, 0 and I denote the zero matrices and the identity matrix, respectively.

2. Problem Statement

2.1. Study System Model

The study system is a nonlinear load (harmonic producing element) connected in parallel with APF. Both are connected to a large grid at the point of common coupling, PCC, as shown in Figure 1. The large utility grid is represented by its equivalent Thevenin constant voltage source in series with reactance L_g. The nonlinear load is represented by an injected current source i_L contaminated with harmonics. The single-phase nonlinear load is depicted in Figure 2, and all components' values (system parameters) are given in Table 1.

The main function of the shunt active power filter (SAPF) is to inject an equal but opposite harmonic compensating current to compensate for current harmonics. This means that SAPF acts as a current source that injects 180° phase-shifted harmonic components generated by the load. As a result, components of harmonic currents contained in the load current are canceled by SAPF, and the grid current remains sinusoidal. Note that the current injected by a grid-following converter is regulated with a precise phase displacement from the grid voltage at the point of common connection (PCC). As a result, knowledge of the grid voltage's fundamental frequency phasor is available all the time for the accurate calculation of the converter's reference current, amplitude, and angle with respect to the grid voltage phasor. Outer control loops modify this to inject the needed amount of active and reactive power, as well as the RMS control voltage.

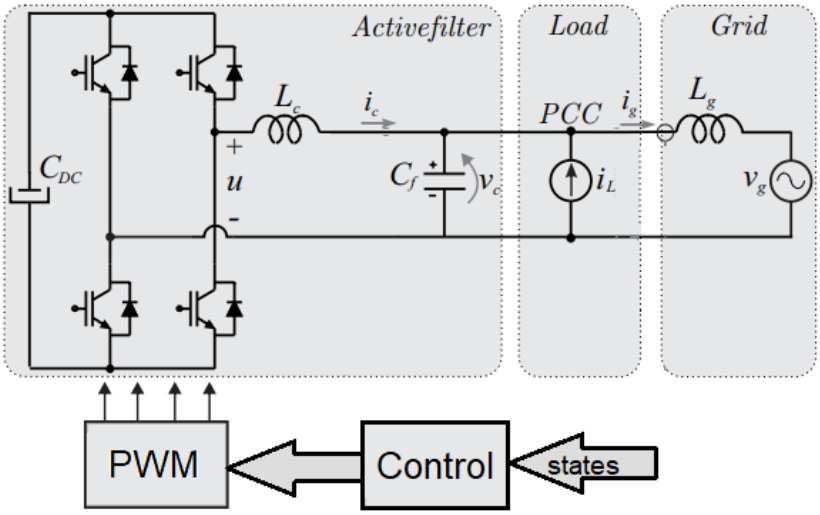

Figure 1. Nonlinear load and shunt APF connected to the grid at the PCC.

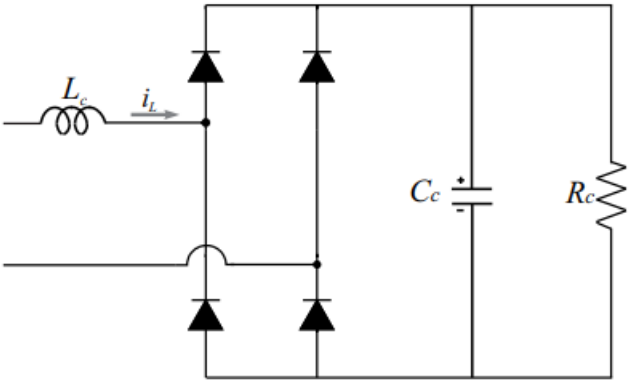

Figure 2. Single-phase standard nonlinear load (Rectifier load). Note that there is no restriction on the value of R_c.

Table 1. Parameters of the system under study.

Parameter	Value
Converter Inductance L_c	1 mH
Filter Capacitor C_f	62 µF
Max. grid inductance L_{gmax}	1.5 mH
Min. grid inductance L_{gmin}	0.5 mH
Load inductance L_c	10 mH
Load capacitor C_c	0.1 mF
Load resistor R_c	50 Ω

The active filter is fitted near the source of harmonics in a radial power distribution feeder so that it effectively attenuates the harmonics throughout the feeder.

Applying Kirchhoff's laws, the study system can be modeled as follows:

$$\begin{aligned} L_c \frac{di_c}{dt} &= u - v_c \\ L_g \frac{di_g}{dt} &= v_c - v_g \\ \dot{v}_c &= \frac{1}{C_f}(-i_g + i_L + i_c) \end{aligned} \tag{1}$$

The parameters' meanings and values of (1) are given in Table 1. For small deviations around an operating point, the state vector and the external disturbances may be defined as:

$$x = \begin{bmatrix} \Delta i_c & \Delta i_g & \Delta v_c \end{bmatrix}', \; w = \Delta i_L$$

The Linearized model, considering $v_g =$ constant, gives the state equation:

$$\dot{x} = \begin{bmatrix} 0 & 0 & \frac{-1}{L_c} \\ 0 & 0 & \frac{1}{L_g} \\ \frac{1}{C_f} & \frac{-1}{C_f} & 0 \end{bmatrix} x + \begin{bmatrix} \frac{1}{L_c} \\ 0 \\ 0 \end{bmatrix} u + \begin{bmatrix} 0 \\ 0 \\ \frac{1}{C_f} \end{bmatrix} w, \; z = \begin{bmatrix} 0 & 1 & 0 \end{bmatrix} x \tag{2}$$

where z is the variable to be optimized. Equation (2) can be written as:

$$\begin{array}{c} \dot{x} = Ax + Bu + Dw, \\ y = C_y x, \; C_y = [0\,1\,0] \\ z = C_z x, C_y = C_z = C \end{array} \tag{3}$$

where the vectors $x(t) \in R^n$, $u(t) \in R^m$, $y(t) \in R^l$, $w(t) \in R^p$, $z(t) \in R^r$ are, respectively, the states, control, output for feedback, the external disturbance (perturbation), and the output to optimize. The system matrices are:

$$A = \begin{bmatrix} 0 & 0 & \frac{-1}{L_c} \\ 0 & 0 & \frac{1}{L_g} \\ \frac{1}{C_f} & \frac{-1}{C_f} & 0 \end{bmatrix}, \; B = \begin{bmatrix} \frac{1}{L_c} \\ 0 \\ 0 \end{bmatrix}, \; D = \begin{bmatrix} 0 \\ 0 \\ \frac{1}{C_f} \end{bmatrix}, C_y = C_z = C = \begin{bmatrix} 0 & 1 & 0 \end{bmatrix}$$

The pairs (A, B) and (A, C_y) are controllable and observable, respectively. Note that y is equal to the grid current Δi_g. Note that in the above model, the time delay is neglected because the system is very fast.

2.2. Problem Formulation

It is required to design a state feedback controller:

$$u = Kx \tag{4}$$

such that the injected current to the grid i_g be as clean as possible and under different topology changes of the grid (represented by uncertainty in L_g).

To obtain a clean grid current, i_g has to follow a sinusoidal reference *r(t)*. Following a time-varying reference is termed a tracking problem. This is carried out by minimizing the error.

$$e = r - y \, . \tag{5}$$

3. Problem Solution

3.1. Augmented System

Because the system has no integrator (system type 0), there will be a steady-state error for a step input, according to the system model (3). As a result, as shown in Figure 3, the plant system order must be increased by inserting an integrator.

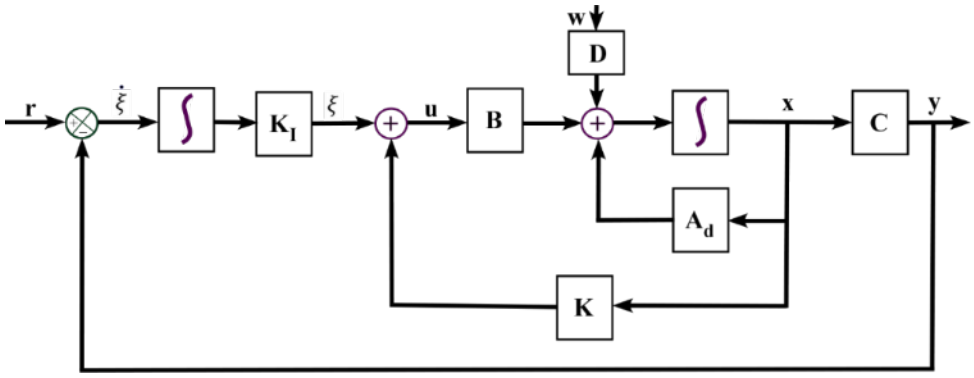

Figure 3. Tracking system.

The control objective is to minimize the effect of grid reactance changes on the output voltage of the study system by rejecting the harmonics. The output voltage is also used for feedback, so C_y is chosen equal to $C_z = C$. The dynamic tracker, state feedback with integral control, is suggested as follows:

$$u = Kx + K_I\xi, \dot{\xi} = r - Cx \tag{6}$$

The augmented system's closed-loop is given by:

$$\begin{bmatrix} \dot{x} \\ \dot{\xi} \end{bmatrix} = \begin{bmatrix} A + BK & BK_I \\ -C & 0 \end{bmatrix} \begin{bmatrix} x \\ \xi \end{bmatrix} + \begin{bmatrix} D \\ 0 \end{bmatrix} w + \begin{bmatrix} 0 \\ I \end{bmatrix} rz = \begin{bmatrix} C & 0 \end{bmatrix} \begin{bmatrix} x \\ \xi \end{bmatrix} + B_2 u \tag{7}$$

$$subject\ to\ w'w \leq 1$$

Or,

$$\begin{bmatrix} \dot{x} \\ \dot{\xi} \end{bmatrix} = (\hat{A} + \hat{B}\hat{K}) \begin{bmatrix} x \\ \xi \end{bmatrix} + \hat{D}w + \begin{bmatrix} 0 \\ I \end{bmatrix} r, z = \hat{C} \begin{bmatrix} x \\ \xi \end{bmatrix} + B_2 u,$$

$$subject\ to\ w'w \leq 1$$

where the augmented matrices are:

$$\hat{A} = \begin{bmatrix} A & 0 \\ -C & 0 \end{bmatrix}, \hat{B} = \begin{bmatrix} B \\ 0 \end{bmatrix}, \hat{D} = \begin{bmatrix} D \\ 0 \end{bmatrix}, \hat{C} = \begin{bmatrix} C & 0 \end{bmatrix}, \hat{K} = [K, K_I] \tag{8}$$

Note that the term B_2u is added to the output z to avoid a large control signal, which is undesired in practice. Also, the normalized bounded norm of the external disturbance w, $\|w(t)\|^2 = w'w \leq 1, t \geq 0$, can always be achieved by proper selection of D.

For example, if the original system has $Dw \leq 2$, then selecting $D_{new} = \frac{1}{2}D$ results in satisfying the constraint $w'w \leq 1$.

3.2. The Invariant (or Attracting) Ellipsoid Set

The invariant (or attracting) ellipsoid design has recently been developed in robust control of linear and nonlinear systems [21]. Moreover, the ellipsoidal design is successfully applied in many applications, e.g., automatic generation control [22], piezoelectric actuators [23], car active suspension [24], islanded AC [25,26], and hybrid microgrids [27]. For a positive definite matrix $0 < P = P' \in R^{n+l}$ introduce the Lyapunov (or energy) function [28],

$$V = \begin{bmatrix} x \\ \xi \end{bmatrix}' P^{-1} \begin{bmatrix} x \\ \xi \end{bmatrix} \leq 1 \tag{9}$$

This quadratic function can also be interpreted as an ellipsoid set, E, centered at the origin.

The following two requirements are the basic ideas of the ellipsoidal-based control:

(1) For an initial state vector outside of the ellipsoid, the state trajectory must be attracted to the ellipsoidal set, including the origin (attracting ellipsoid);

(2) The trajectory will not leave the ellipsoid once it reaches it (invariant set).

These require that $\dot{V} \leq 0$ *subject to* $V \geq 1$, *and* $w'w \leq 1$. Or along with ((7),(8)) and let $Q = P^{-1}$ gives,

$$\begin{bmatrix} x \\ \xi \end{bmatrix}' \left(Q\hat{A} + Q\hat{B}\hat{K} + *\right) \begin{bmatrix} x \\ \xi \end{bmatrix} + 2w'\hat{D}'Q \begin{bmatrix} x \\ \xi \end{bmatrix} \leq 0, s.t. V \geq 1, \text{ and } w'w \leq 1 \tag{10}$$

The last two constraints can be combined into one using the S-procedure, [21]. Equation (10) is satisfied if the following equation is fulfilled:

$$\begin{bmatrix} x \\ \xi \\ w \end{bmatrix}' \begin{bmatrix} \left(\hat{A}P + \hat{B}Y + *\right) + \alpha P & \hat{D} \\ * & -\alpha I \end{bmatrix} \begin{bmatrix} x \\ \xi \\ w \end{bmatrix} \leq 0 \tag{11}$$

for a scalar, $\alpha > 0$. Where $Y = \hat{K}P$, and (3) to reduce the external disturbance effect on the system response and to stabilize the dynamic system (7) in a small enough vicinity of the origin, the ellipsoid volume must be minimized. For this, the ellipsoid E, (9), for the augmented vector is replaced by:

$$E_z = z'((\hat{C} + B_2\hat{K})P(\hat{C} + B_2\hat{K})')^{-1}z \leq 1 \tag{12}$$

for the output z. This ellipsoid is bounding the output z. To minimize the impact of the external disturbance w on the output z, the volume of the ellipsoid E_z has to be minimized. This is why adding the term B_2u in (7) results in a small control signal. Substituting for z from (6), (7), one gets $z = (C + B_2K)x + B_2K_I\xi$. Due to the changes in the large grid topology, L_g, changes. Therefore, the $\hat{A}$ matrix in (11) is replaced by $\hat{A} + \Delta\hat{A}$, The uncertainty is represented in the norm-bounded form, $\Delta\hat{A} = M\Delta(t)N$, $\|\Delta(t)\| \leq 1$.

The following theorem determines the controller.

Theorem 1. *Assume that the system (7), is controllable* $\left(\hat{A}, \hat{B}\right)$*, and observable* $\left(\hat{A}, \hat{C}\right)$*, under L∞-bounded exogenous disturbances. Then, the robust disturbance-rejection state feedback plus integral controller is obtained by solving:*

$$minimize\ trace\left[\hat{C}P\hat{C}' + \left(B_2Y\hat{C}' + *\right) + B_2ZB_2'\right] \tag{13}$$

$$s.t. \begin{bmatrix} \left(\hat{A}P + \hat{B}Y + *\right) + \alpha P + \epsilon MM' & \hat{D} & PN' \\ * & -\alpha I & 0 \\ * & * & - \in I \end{bmatrix} \leq 0, \begin{bmatrix} Z & Y \\ * & P \end{bmatrix} \geq 0, \ P > 0 \tag{14}$$

Note that, due to its linearity, the trace function is used. The minimization is carried out to the variables α, $P = P' > 0, Y, Z$. Note that the product term αP is a source of nonlinearity in the above matrix equations. This difficulty can be removed by fixing α. The resulting equations will become LMIs. The minimization is done through iterations on α.

3.3. The Proposed Controller

The above LMIs (13) are solved using yalmip interface and sedumi solver. The following gain matrices of the proposed controller are: K = [−8.3923 2.2162 −1.953], Ki = 2692.3.

4. Simulation and Experimental Validation

4.1. Simulation Validation

MATLAB/SimPowerSystems Toolbox is used to test and simulate the proposed shunt Active Power Filter (APF) connected to the grid with a nonlinear load. To verify the robustness of the proposed control, five test cases are achieved. In case (1), the grid current is tested and compared without and with controlled APF. The proposed controller shows the advantage of using shunt APF. In case (2), the grid current is checked using harmonic spectra as a percentage of the fundamental component of the grid current against varying the load current from 25% to 150% of the rated value. In case (3), the proposed system with invariant set controlled APF is tested against an unbalanced nonlinear load. In case (4), the proposed controller grid current is checked against grid parameters uncertainty (L_g is varied from 50% to 150 % of the rated value). Finally, in case (5) the proposed controller has tested against the distorted grid and grid parameters uncertainty. In this case, the proposed controller is compared with H∞ robust controller [29].

Case (1): Comparison between, without, and with controlled shunt APF

In this case, the proposed system is tested without and with a controlled APF. The invariant set controller is used to regulate the grid currents. Figure 4 shows the grid phase-current without controlled APF in (a, b) and with controlled APF in (c, d). Figure 4a shows the grid current waveform without controlled APF, and the respected harmonic spectra are given in Figure 4b. The Total Harmonic Distortion (THD) for this case is 15.57% (disagreeing with IEEE 1547 standard [30]). While Figure 4c shows the grid current waveform with controlled APF, and the respected harmonic spectra are given in Figure 4d, the Total Harmonic Distortion (THD) for this case is 1.58% (which agrees with IEEE 1547 Standard [30]).

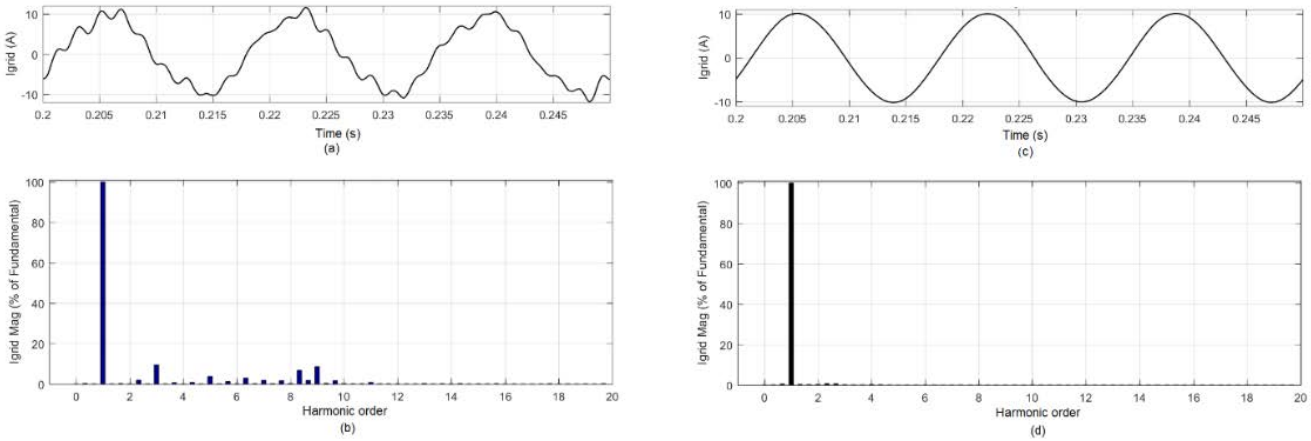

Figure 4. The grid phase-current waveform and the harmonics contents (**a**,**b**) without control and (**d**,**c**) with the invariant set controller.

Tables 2 and 3 show the odd harmonic grid current distortion in percent of the fundamental component without and with APF, respectively. The given results show that it is a must to use a controlled APF to tackle this problem. Meantime, the invariant set controller gives much lower THD compared to the H∞ controller used in [31], which is 5.27% (disagreeing with IEEE 1547 standard).

Table 2. Odd harmonic grid current distortion in percent of the fundamental component without APF.

Harmonic Component	Percentage
Fundamental	100%
h = 3	9.47%
h = 5	0.06%
h = 7	1.77%
h = 9	8.58%
h = 11	0.87%
h = 13	0.3%
h = 15	0.07%
h = 17	0.03%
h = 19	0.04%

Table 3. Odd harmonic grid current distortion in percent of the fundamental component with APF.

Harmonic Component	Percentage
Fundamental	100%
h = 3	0.97%
h = 5	0.24%
h = 7	0.24%
h = 9	0.04%
h = 11	0.02%
h = 13	0.01%
h = 15	0.01%
h = 17	0.01%
h = 19	0.00%

Table 4 provides a summary of the situations for 25%, 50%, 100%, and 150% of the rated load, respectively case (1). It demonstrates the degree to which the proposed system, with or without a tracker, matches or mismatches the IEEE 1547 THD standard for 25%, 50%, 100%, and 150% of the rated load.

Table 4. THD and agree/disagree with IEEE 1547 standard without and with controlled APF against load changes.

Nonlinear Load		Without Controlled APF		With the Proposed APF Control
Load	THD	Agree with IEEE 1574?	THD	Agree with IEEE 1574?
25%	7.65%	No	0.47%	Yes
50%	9.39%	No	0.97%	Yes
100%	15.57%	No	1.58%	Yes
150%	25.95%	No	2.78%	Yes

Case (2): Comparison between without and with controlled shunt APF during load changes

The proposed system shown in Figure 1 has been tested by varying the nonlinear load current in steps as a percentage of the rated load without and with controlled APF. Figure 5 shows the Harmonic spectra and the limits of IEEE 1547 Standard for the grid current without and with control under 25%, 50%, 100%, and 150% rated loads. The results illustrate that the proposed system without controlled APF has THD higher than 5% and disagrees with the IEEE 1547 Standard, while with proposed controlled APF in all the load change cases, the THD is much less (5%) and all four cases agree with IEEE 1547 Standard. Table 4 illustrates the THD in all cases, with and without controlled APF, and if it agrees/disagrees with the IEEE 1547 standard.

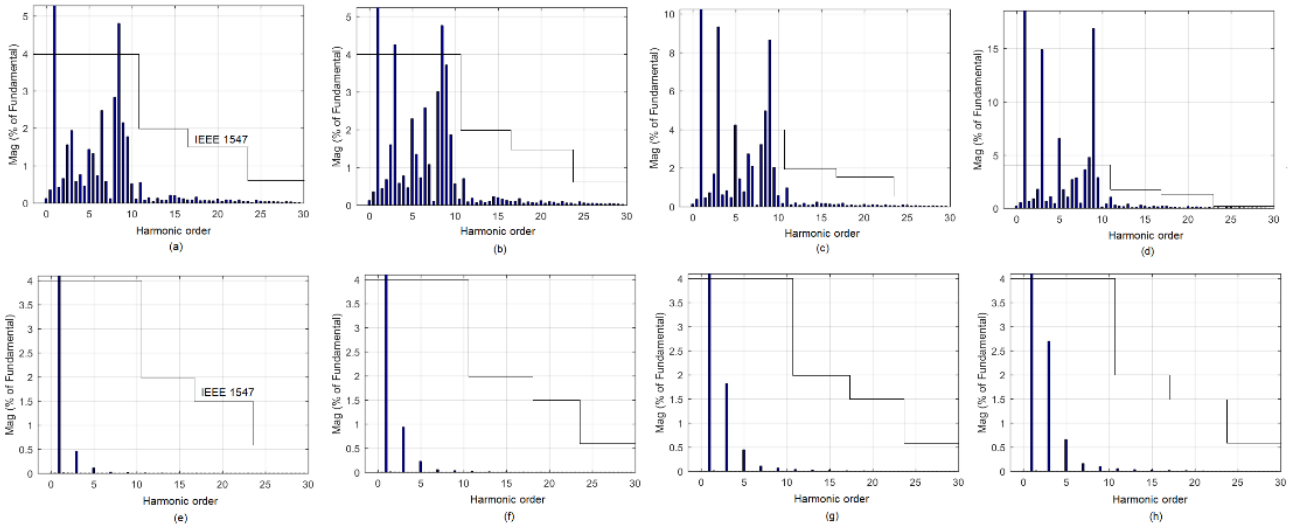

Figure 5. Harmonic spectra and the limits of IEEE 1547 Standard for the grid currents without and with control under 25%, 50%, 100%, and 150% rated loads, (**a**–**d**) without control, and (**e**–**h**) with control.

Case (3): Unbalanced Nonlinear Load

A three-phase system with a nonlinear load (three-phase rectifier load) is used to test the proposed technique under a very severe condition. The three-phase proposed system (Figure 1 is the single-phase version) is tested with an unbalanced three-phase nonlinear load. In Figure 6, at t = 0.2 s, the three-phase load changes from a balanced load to an unbalanced load. The three-phase unbalanced loads applied are 80% phase A, 100% phase B, and 60% phase C, as shown in Figure 6a. The three-phase grid currents are given in Figure 6b, as well as the harmonic spectra of the three-phases of the grid currents (Phase A in (c), Phase B in (d), and Phase C in (e)) and limits of IEEE 1547 Standard. The results prove that the proposed system with invariant set controlled APF has THD much less than 5% and agrees with the IEEE 1547 Standard. The THD for the three-phases of the grid current while unbalanced are: THD-phase A = 1.72%, THD-phase B = 2.67%, and THD-phase C = 1.39%). All phases agree with the IEEE 1547 Standard.

Case (4): Uncertainty in the grid parameters

To determine the ability to track sinusoidal references, Figure 7a,b demonstrates, for both cases of extreme values of grid inductance (L_{gmin}, and L_{gmax}), the grid currents. It is clearly shown that, even with the load currents (100% of rated value) with harmonics, the grid currents provided by the invariant set control system have very low distortion and low harmonic content and agree with the IEEE 1547 Standard. Moreover, the THD with L_{gmin} is 0.87%, and the THD with L_{gmax} is 2.37%. Case (5) shows the superiority of the proposed controller as compared to the H_∞ controller [29].

After injecting grid currents, the proposed and H∞ controllers are tested for adherence with IEEE 1547 criteria for individual harmonics and THD. As demonstrated in Table 5, both controllers operate accurately even when the grid impedance is uncertain. Furthermore, our proposal outperforms the H∞ controller.

The H∞ is one of the most effective methods for rejecting disturbances, however, the degree of rejection slows down the system response. In the proposed method, this condition does not exist. The degree of disturbance rejection is greater than H ∞ when the system response is much faster than H∞. This is one of the outstanding features of the proposed method.

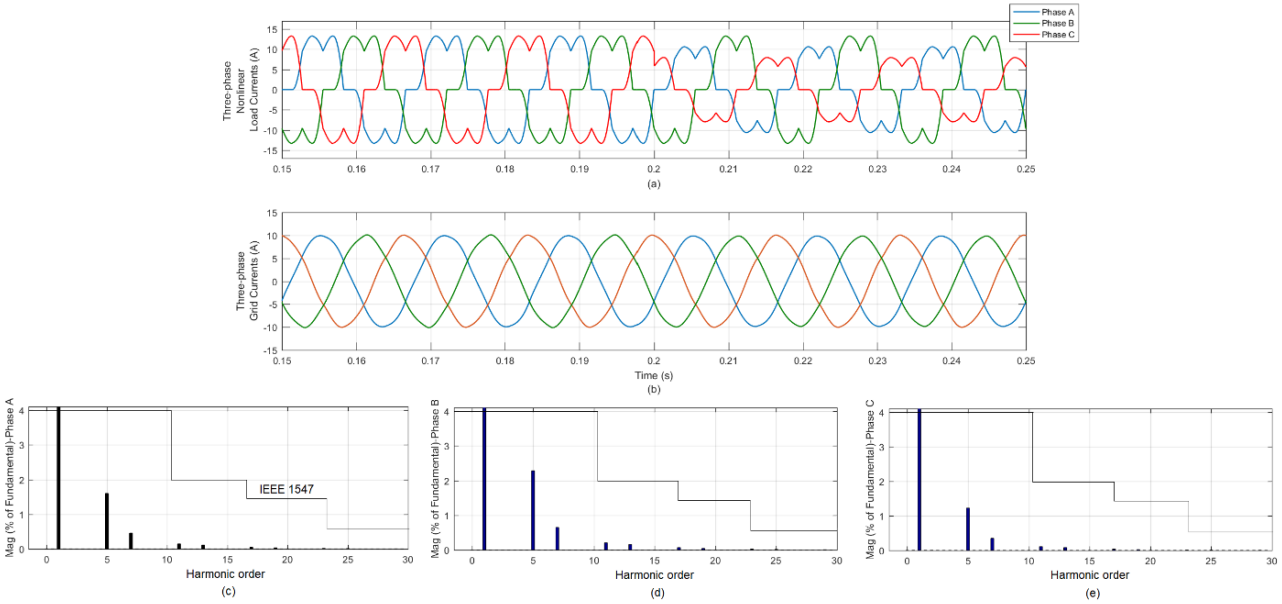

Figure 6. (**a**) Three-phase inductors current, (**b**) three-phase grid current, (**c**,**d**) of the three-phases of the grid currents (Phase A in (**c**), Phase B in (**d**), and Phase C in (**e**)) and the limits of IEEE 1547 Standard during unbalanced nonlinear load.

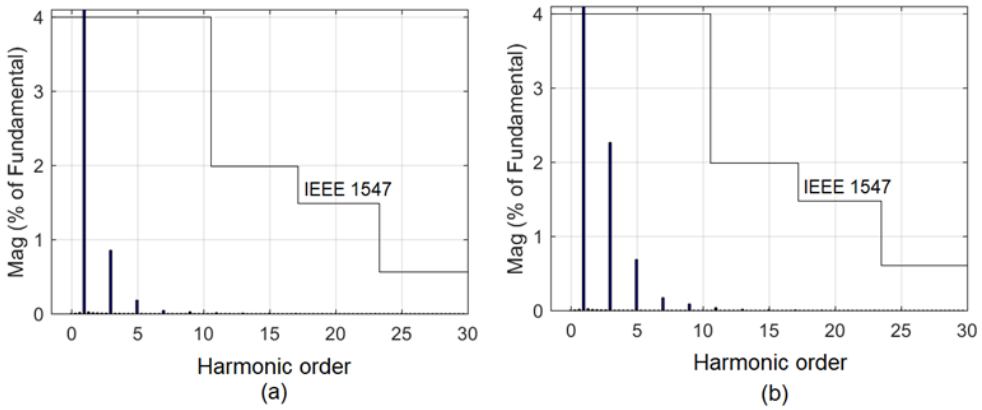

Figure 7. Harmonic spectra and the limits of IEEE 1547 Standard for the grid currents with invariant control at 100% load with uncertainty in the grid inductance; (**a**) with L_{min}, and (**b**) with L_{max}.

Table 5. Comparing THD using the suggested controller and the H∞ controller at L_{gmin} and L_{gmax}.

	Invariant Sets Controller		**H∞ Controller [29]**	
	L_{gmin}	L_{gmax}	L_{gmin}	L_{gmax}
THD	0.87%	2.37%	1.13%	2.87%

Case (5): Distorted Grid voltage and uncertainty in grid parameters

Consider a grid distorted voltage with 3rd, 5th, and 7th harmonic components with amplitudes of 5%, 6%, and 5% of the fundamental, respectively, to verify that the invariant set controller can effectively attenuate harmonics [32]. A comparison between the proposed controller and the H∞ controller in [29] is given in this section when the system is opposing a grid-distorted voltage and uncertainty in the grid parameters (L_{gmin}, and L_{gmax}). Figures 8 and 9 show the three-phase grid current waveform and the respective harmonic spectra during distorted grid voltage and with L_{gmin} and L_{gmax}, respectively.

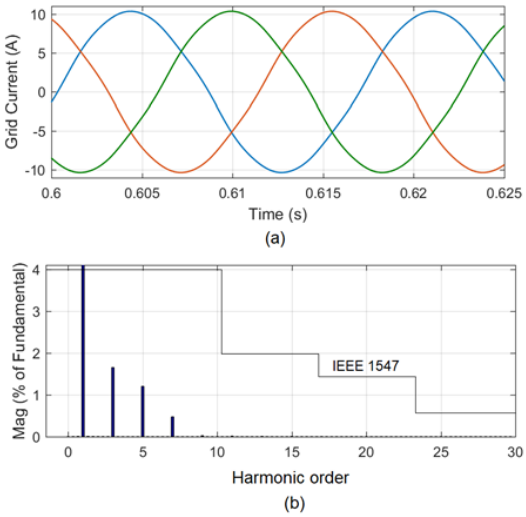

Figure 8. Three-phase grid current waveform and the respective harmonic spectra during distorted grid voltage and with L_{gmin}. for the proposed controller.

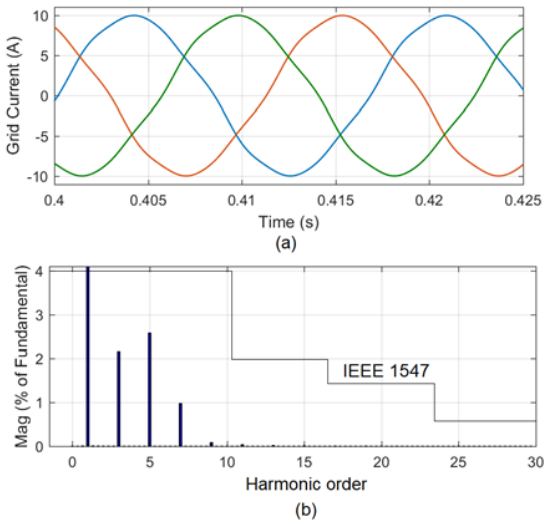

Figure 9. Three-phase grid current waveform and the respective harmonic spectra during distorted grid voltage and with L_{gmax} for the proposed controller.

In Figures 8a and 9a the three-phase grid current waveform of the proposed controller during distorted grid voltage and with L_{gmin} and L_{gmax}, respectively, while the three-phase current waveform of the H∞ controller is shown in [29].

In Figures 8b and 9b, the harmonic spectra and the limits of IEEE 1547 Standard for the grid current of the proposed controller during distorted grid voltage and with L_{gmin} and L_{gmax}, respectively, while in [29] the harmonic spectra and the limits of IEEE 1547 Standard for the grid current of the H∞ controller.

Both controllers are tested for compliance with IEEE 1547 requirements for individual harmonics and THD after injecting grid currents. As shown in Table 6, both controllers are working accurately even with uncertainty in the grid impedance and harmonics in the grid voltage.

Table 6. Comparing the distorted voltage grid's THD using the suggested controller and the H∞ controller at L_{gmin} and L_{gmax}.

	Invariant Set Controller		**H∞ Controller [29]**	
	Distorted voltage grid + L_{gmin}	Distorted voltage grid + L_{gmax}	Distorted voltage grid + L_{gmin}	Distorted voltage grid + L_{gmax}
THD	2.04%	3.27%	2.22%	3.29%

4.2. Experimental Validation

4.2.1. Experimental Setup

The experimental setup involved a single-phase nonlinear load that is fed by a reduced grid voltage via a step-down transformer, a current sensor, and a data acquisition system, as shown in Figure 10. In this setup, a DAQ card NI PCIe-6323 with 32 Analog Input, 48 Digital I/O, 4 Analog Outputs, and 250 kS/s single-channel sampling rate was used. This data acquisition system was used to read the real inductor current to be fed to the developed controller under the simulation environment. In this experiment, a sampling rate of 0.5 msec and an input voltage level of −10 to 10 Volts were used.

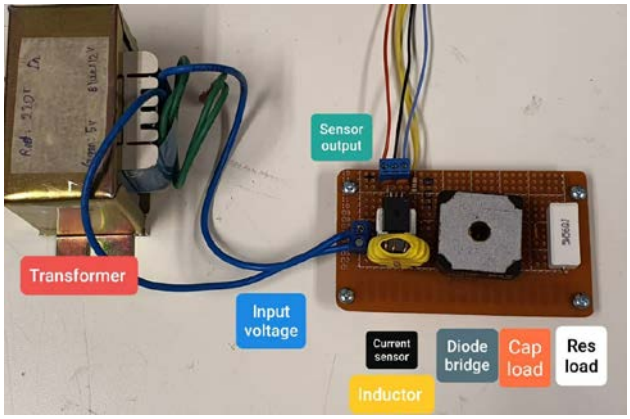

(**a**)

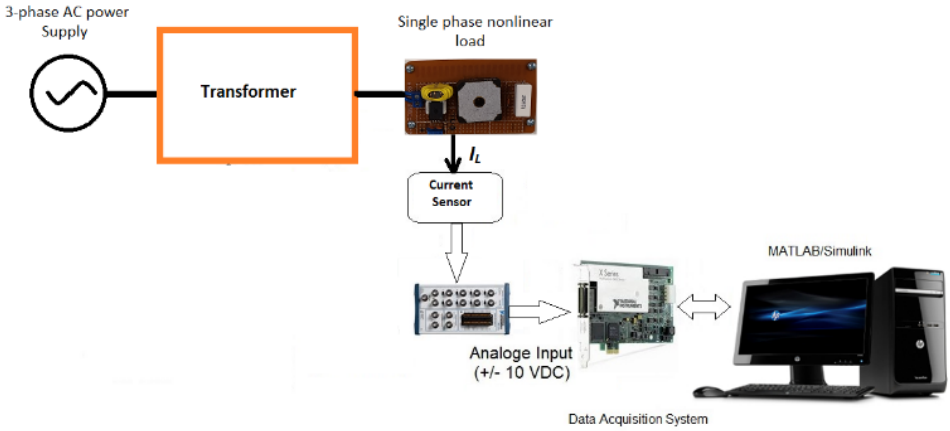

(**b**)

Figure 10. *Cont.*

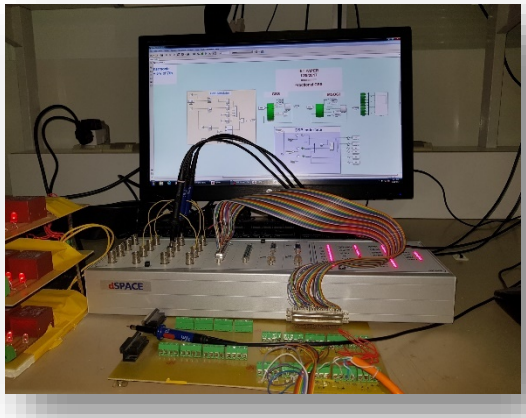

(**c**)

Figure 10. (**a**) Real circuit of the single-phase nonlinear load, (**b**) schematic diagram of the experimental setup, (**c**) real-time experimental setup.

The inductor and grid current and voltage values are measured and sensed via a data acquisition system. The stored files in the data acquisition system are then imported to the MATLAB environment and then exported to a MATLAB workspace to be plotted with the same sampling time used in the data acquisition system.

4.2.2. Experimental Results

To investigate the robustness of the proposed controller, the single-phase proposed system shown in Figure 10 is tested without the controller (open-loop) at 100% load. Figure 11 shows open- loop real measurement of input voltage, inductor voltage, and inductor current. Note that open(closed)-loop means without(with) using the proposed tracker. The real grid current is measured through the current sensor.

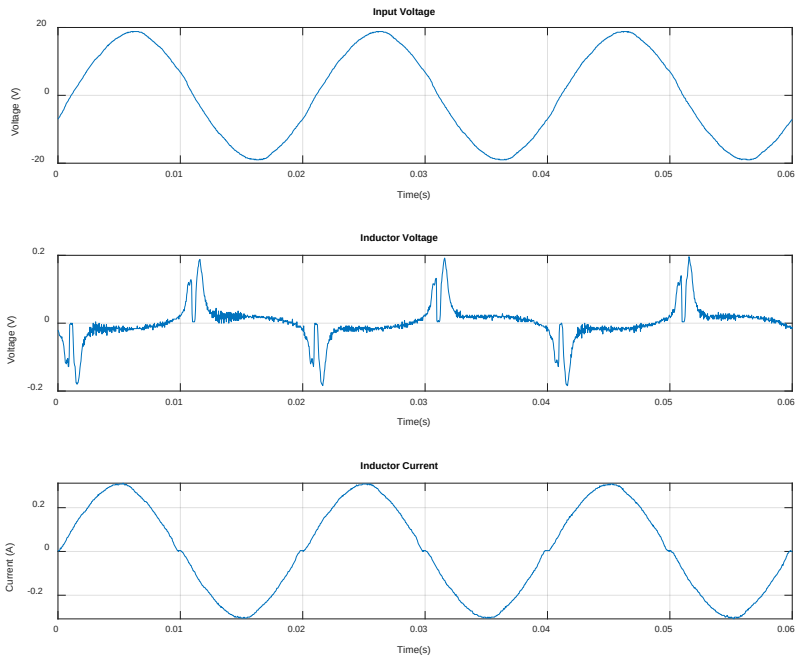

Figure 11. Open loop measurement of real input voltage, inductor voltage, and inductor current.

The grid current and inductor current are given in Figure 12a. The THD of the grid current is 20.38%. Figure 12b shows the spectrum analysis of I_{grid} without control.

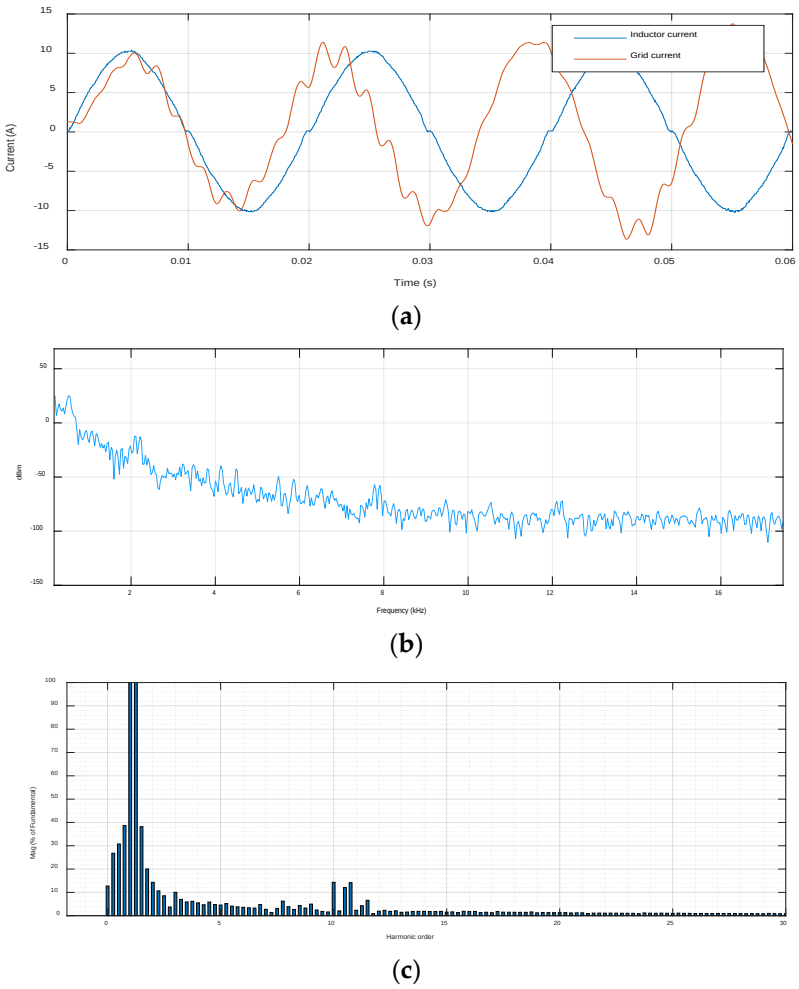

(**a**)

(**b**)

(**c**)

Figure 12. System response without control: (**a**) I_{grid} vs. I_L with THD_I_{grid} = 20.38%, (**b**) spectrum analysis of I_{grid}, (**c**) Harmonics contents of I_{grid}.

Meanwhile, the harmonics contents as a percentage of the fundamental of I_{grid} without control are given in Figure 12c. However, the THD is quite high; we chose a load that reflects this excessive distortion to the grid current to evaluate the proposed regulation. It can filter out most of this distortion and generate an output that conforms to the IEEE1547 standard. This means that it will perform perfectly under any actual grid main current distortion.

The proposed controller is tested and evaluated through the result findings in Figure 13. Figure 1 depicts the circuit diagram required to calculate the results seen in Figure 13. Using a data acquisition system, the inductor and grid current and voltage values are measured. The data acquisition system's stored files are then imported into the MATLAB environment and exported to a MATLAB workspace for plotting using the same sampling time as the data acquisition system.

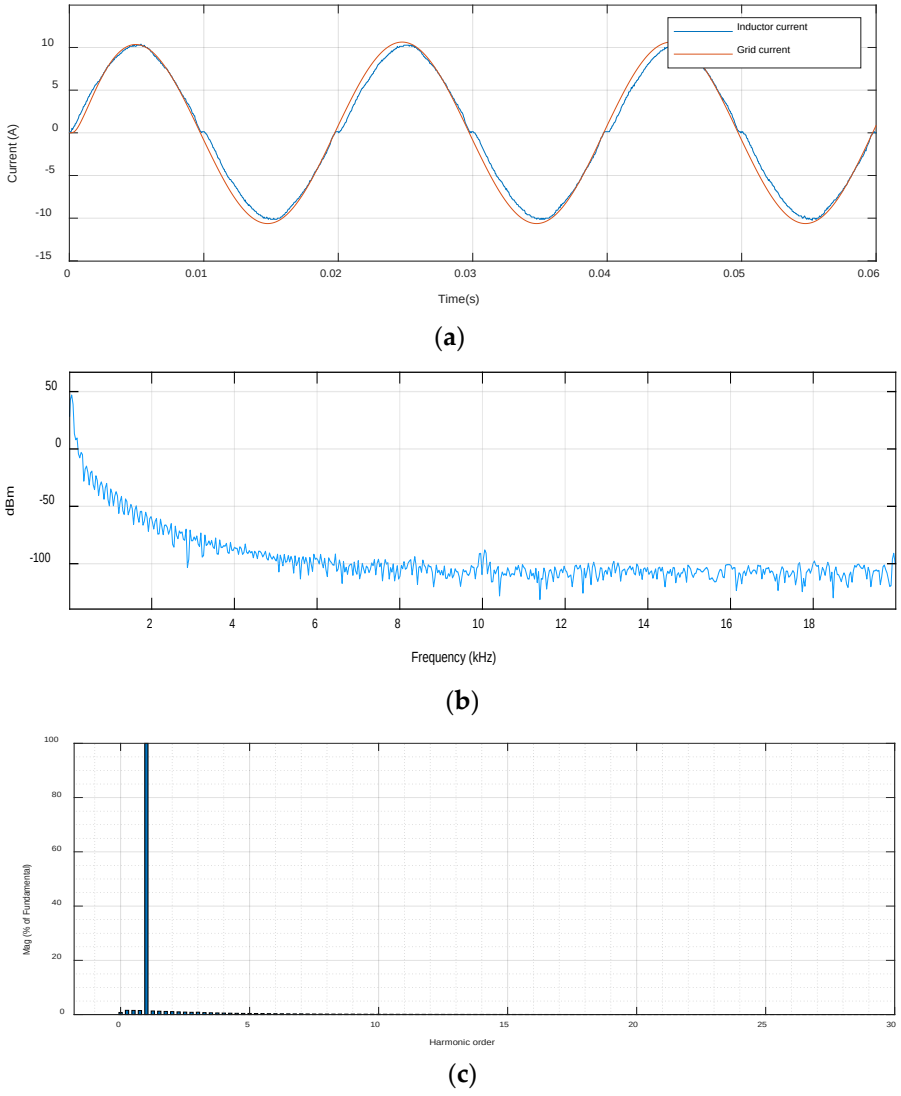

Figure 13. System response with control: (**a**) I_{grid} vs. I_L with THD_I_{grid} = 1.747%, (**b**) spectrum analysis of I_{grid}, (**c**) Harmonics contents of I_{grid}.

The grid current and inductor current are shown in Figure 13a. The THD of the grid current is 1.747%. Figure 13b illustrates the spectrum analysis of I_{grid} with the proposed control. In the meantime, the harmonics contents as a percentage of the fundamental of I_{grid} with the invariant set control are given in Figure 13c.

The simulation and experimental tests prove that the proposed controller has reduced the THD of the grid current from a very high percentage (20.38% in practical results) which does not agree with the IEEE 1547 standard (5%) to a very low percentage (1.747% in practical). Note that adding L between the filter capacitor and the nonlinear load will help to decrease the harmonic contents, but the proposed APF succeeded in doing the job perfectly without using that.

5. Conclusions

In this paper, the ellipsoidal design to solve a regulator problem (for constant reference) is extended to solve a tracking problem (time-varying reference). The study system considered in this work is a grid system with a nonlinear load and variable inductance. The system is represented by the state-space model, the nonlinear load is modeled as a current disturbance, and the grid inductance variation is cast into the norm-bounded form. The attracting ellipsoid method (AEM) and LMI optimization was used to design a controller

that is robust against changes in the grid topology. The proposed robust control attenuates the effect of the harmonics-producing nonlinear load on the grid current. It is also capable of tracking the sinusoidal reference for the grid current, in addition to ensuring stability for the grid inductance changes. Simulation and experimental results show compliance with the IEEE standard 1547.

Future work is applying the synergetic control approach [33] and AI methods [34,35] to increase the robustness and invariance of the worst external disturbances.

Author Contributions: Methodology, H.M.S., E.H.E.B.; software, A.S. and E.H.E.B.; validation, H.M.S. and M.D.S.; data curation, E.H.E.B. and M.D.S.; writing—review and editing, H.M.S., A.S., E.H.E.B. and M.D.S.; visualization, A.S.; supervision, H.M.S. All authors have read and agreed to the published version of the manuscript.

Funding: This research received no external funding.

Institutional Review Board Statement: Not applicable.

Informed Consent Statement: Not applicable.

Data Availability Statement: Not applicable.

Conflicts of Interest: The authors declare no conflict of interest.

References

1. Beltran-Carbajal, F.; Tapia-Olvera, R.; Valderrabano-Gonzalez, A.; Yanez-Badillo, H. An Asymptotic and Algebraic Estimation Method of Harmonics. *Electr. Power Syst. Res.* **2022**, *206*, 107771. [CrossRef]
2. *IEEE:1547.6*; Standard for Interconnecting Distributed Resources with Electric Power Systems. IEEE: Piscataway, NJ, USA, 2011.
3. Akagi, H. Active Harmonic Filters. *Proc. IEEE* **2005**, *93*, 2128–2141. [CrossRef]
4. Toufik, T.; Ahmed, A.; Abdelmalek, M.; Othmane, A.; Abdallah, B.; Mouloud, D. Robust control of series active power filters for power quality enhancement in distribution grids: Simulation and experimental validation. *ISA Trans.* **2022**, *107*, 350–359.
5. Peña-Alzola, R.; Liserre, M.; Blaabjerg, F.; Sebastián, R.; Dannehl, J.; Fuchs, F.W. Analysis of the Passive Damping Losses in LCL-Filter-Based Grid Converters. *IEEE Trans. Power Electron.* **2013**, *28*, 2642–2646. [CrossRef]
6. Beres, R.N.; Wang, X.; Blaabjerg, F.; Liserre, M.; Bak, C.L. Optimal Design of High-Order Passive-Damped Filters for Grid-Connected Applications. *IEEE Trans. Power Electron.* **2016**, *31*, 2083–2098. [CrossRef]
7. Wang, X.; Blaabjerg, F.; Loh, P.C. Grid-Current-Feedback Active Damping for LCL Resonance in Grid-Connected Voltage-Source Converters. *IEEE Trans. Power Electron.* **2016**, *31*, 213–223. [CrossRef]
8. Bayoumi, E.H.E. Design of Three-Phase LCL-Filter for Grid-Connected PWM Voltage Source Inverter Using Bacteria Foraging Optimization. In *Electricity Distribution: Intelligent Solutions for Electricity Transmission and Distribution Networks*; Springer: Berlin/Heidelberg, Germany, 2016; pp. 199–219.
9. Pan, D.; Ruan, X.; Bao, C.; Li, W.; Wang, X. Optimized Controller Design for LCL-Type Grid-Connected Inverter to Achieve High Robustness Against Grid-Impedance Variation. *IEEE Trans. Ind. Electron.* **2015**, *62*, 1537–1547. [CrossRef]
10. Hanif, M.; Khadkikar, V.; Xiao, W.; Kirtley, J.L. Two Degrees of Freedom Active Damping Technique for LCL Filter-Based Grid Connected PV Systems. *IEEE Trans. Ind. Electron.* **2014**, *61*, 2795–2803. [CrossRef]
11. Xu, J.; Xie, S.; Tang, T. Active Damping-Based Control for Grid-Connected LCL-Filtered Inverter With Injected Grid Current Feedback Only. *IEEE Trans. Ind. Electron.* **2013**, *61*, 4746–4758. [CrossRef]
12. Boyd, S.; El Ghaoui, L.; Feron, E.; Balakrishnan, V. *Linear Matrix Inequalities in System and Control Theory*; SIAM Studies in Applied Mathematics: Philadelphia, PA, USA, 1994.
13. De Oliveira, M.C.; Geromel, J.C.; Bernussou, J. Extended H 2 and H norm characterizations and controller parametrizations for discrete-time systems. *Int. J. Control.* **2002**, *75*, 666–679. [CrossRef]
14. Maccari, L.A.; Massing, J.R.; Schuch, L.; Rech, C.; Pinheiro, H.; Oliveira, R.C.L.F.; Montagner, V.F. LMI-Based Control for Grid-Connected Converters With LCL Filters Under Uncertain Parameters. *IEEE Trans. Power Electron.* **2013**, *29*, 3776–3785. [CrossRef]
15. Maccari, L.A., Jr.; Santini, A.C.L.; Pinheiro, H.; de Oliveira, R.C.L.F.; Montagner, V.F. Robust optimal current control for grid-connected three-phase pulse-width modulated converters. *IET Power Electron.* **2015**, *8*, 1490–1499. [CrossRef]
16. Zhou, K.; Doyle, J.C.; Glover, K. *Robust and Optimal Control*; Prentice Hall: Upper Saddle River, NJ, USA, 1996.
17. Willmann, G.; Coutinho, D.F.; Pereira, L.F.A.; Libano, F.B. Multiple-loop H1 control design for uninterruptible power supplies. *IEEE Trans. Ind. Electron.* **2007**, *54*, 1591–1602. [CrossRef]
18. Osório, C.R.D.; Koch, G.G.; de Oliveira, R.C.L.F.; Montagner, V.F. A practical design procedure for robust H2 controllers applied to grid-connected inverters. *Control Eng. Pract.* **2019**, *92*, 104157. [CrossRef]
19. Koch, G.G.; Maccari, L.A.; de Oliveira, R.C.L.F.; Montagner, V.F. Robust H∞ State Feedback Controllers based on LMIs applied to Grid-Connected Converters. *IEEE Trans. Ind. Electron.* **2019**, *66*, 6021–6031. [CrossRef]

20. Sun, X.; Cao, J.; Lei, G.; Guo, Y.; Zhu, J. A Robust Deadbeat Predictive Controller with Delay Compensation Based on Composite Sliding Mode Observer for PMSMs. *IEEE Trans. Power Electron.* **2021**, *36*, 10742–10752. [CrossRef]
21. Poznyak, A.; Polyakov, A.; Azhmyakov, V. *Attractive Ellipsoids in Robust Control*; Systems & Control: Foundations & Applications Book Series; Springer International Publishing: Cham, Switzerland, 2014; ISBN 978-3-319-09209-6.
22. Soliman, H.M.; Al-Hinai, A. Robust automatic generation control with saturated input using the ellipsoid method. *Int. Trans. Electr. Energy Syst.* **2018**, *28*, e2483. [CrossRef]
23. Soliman, H.; Saleem, A. Ellipsoidal design of robust tracking controller for large-stroke piezoelectric actuators. *Smart Mater. Struct.* **2020**, *29*, 075031. [CrossRef]
24. Soliman, H.M.; El-Metwally, K.; Soliman, M. Invariant Sets in Saturated and Robust Vehicle Suspension Control. *Arab. J. Sci. Eng.* **2020**, *45*, 7055–7064. [CrossRef]
25. Bayoumi, E.; Soliman, M.; Soliman, H.M. Disturbance-rejection voltage control of an isolated microgrid by invariant sets. *IET Renew. Power Gener.* **2020**, *14*, 2331–2339. [CrossRef]
26. Soliman, H.M.; Bayoumi, E.; Al-Hinai, A.; Soliman, M. Robust Decentralized Tracking Voltage Control for Islanded Microgrids by Invariant Ellipsoids. *Energies* **2020**, *13*, 5756. [CrossRef]
27. Awad, H.; Bayoumi, E.; Soliman, H.; De Santis, M. Robust Tracker of Hybrid Microgrids by the Invariant-Ellipsoid Set. *Electronics* **2021**, *10*, 1794. [CrossRef]
28. Nazin, S.A.; Polyak, B.T.; Topunov, M.V. Rejection of bounded exogenous disturbances by the method of invariant ellipsoids. *Autom. Remote Control* **2007**, *68*, 467–486. [CrossRef]
29. Osorio, C.R.D.; Koch, G.G.; Pinheiro, H.; Oliveira, R.C.L.F.; Montagner, V.F. Robust Current Control of Grid-Tied Inverters Affected by LCL Filter Soft-Saturation. *IEEE Trans. Ind. Electron.* **2019**, *67*, 6550–6561. [CrossRef]
30. Basso, T. IEEE 1547 and 2030 Standards for Distributed Energy Resources Interconnection and Interoperability with the Electricity Grid. National Renewable Energy Laboratory: Golden, CO, USA, 2014.
31. Hornik, T.; Zhong, Q.-C. A Current-Control Strategy for Voltage-Source Inverters in Microgrids Based on H∞ and Repetitive Control. *IEEE Trans. Power Electron.* **2011**, *26*, 943–952. [CrossRef]
32. Teodorescu, R.; Liserre, M.; Rodrıguez, P. *Grid Converters for Photovoltaic and Wind Power Systems*; Wiley: Hoboken, NJ, USA, 2011.
33. Kolesnikov, A.A. Introduction of synergetic control. In Proceedings of the 2014 American Control Conference, Portland, OR, USA, 4–6 June 2014. [CrossRef]
34. Laughton, M.A. Artificial intelligence techniques in power systems. In Proceedings of the IEE Colloquium on Artificial Intelligence Techniques in Power Systems, London, UK, 3 November 1997. [CrossRef]
35. Sumathi, S.; Ashok Kumar, L.; Surekha, P. *Computational Intelligence Paradigms for Optimization Problems Using MATLAB/SIMULINK*; CRC Press: Boca Raton, FL, USA, 2016.